RESEARCH PAPER

Antimicrobial Evaluation of WO_3–TiO_2 Nanocomposites Against Pathogenic Bacterial and Fungal Strains.

T. Kousalya[1], D. Vijayalakshmi[1,*]

[1]Research Scholar, Department of Physics, VELS Institute of Science, Technology & Advanced Studies (VISTAS), Pallavaram, Chennai, Tamil Nadu 600117.

[1]Assistant Professor and Research supervisor, Department of Physics, VELS Institute of Science, Technology & Advanced Studies (VISTAS), Pallavaram, Chennai, Tamil Nadu 600117.*

ABSTRACT

In this study, WO_3/TiO_2 nanocomposites were synthesized and thermally calcined at 800°C and 1200°C to evalute the effect of calcination on structural, optical and antimicrobial perfromance. XRD and FTIR confirmed the formation of mixed-phase crystalline frameworks, while UV-Vis spectroscopy revealed strong visible-light absorption and Tauc plot analysis indicated reduced band gap energies, enhancing antibacterial and antifungal activity. HR-SEM micrograph showed unifromly dispersion spherical nanoparticles with narrow size distribution and minimal agglomeration. The antimicrobial activity of WO_3, TiO_2, and their WO_3/TiO_2 nanocomposites was evaluated against both bacterial and fungal strains. The WO_3/TiO_2 nanocomposites exhibited excellent antibacterial and antifungal activities, with the sample calcined at 1200°C showing significantly higher inhibition zones than the 800°C sample against both bacterial and fungal pathogens. Candida albicans was more susceptible than Aspergillus niger, while strong antibacterial activity was observed against both Gram-positive and Gram-negative bacteria. The enhanced antimicrobial performance is attributed to improved crystallinity, efficient interfacial charge transfer, and increased reactive oxygen species (ROS) generation, resulting in effective disruption of microbial cell membranes. These findings demonstrate that WO_3/TiO_2 nanocomposites are promising eco-friendly materials for antimicrobial coatings, environmental disinfection, and water purification applications.

Keywords: WO_3/TiO_2Nanocomposites, HR-SEM, Antibacterial activity, Gram-positive, Gram-negative

How to cite this article: Katare A, Arya I, Yadav K. Quality of Higher Education in India: Challenges, Opportunities and Future Perspectives. Int J Drug Deliv Technol. 2026;16(71s): 603. DOI: 10.25258/ijddt.16.71s.71

1. Introduction

Nanomaterials have attracted great attention owing to their high surface-to-volume ratio, quantum confinement effects, and tunable physicochemical properties. These features make them promising for application in catalysis, energy conversion, environmental purification, and healthcare. Among them, nanocomposites engineered by integrating multiple material at the nanoscale are particularly promising as they exhibit synergistic effects that enhance photocatalsis, antimicrbial treatment and environmental performance [1-6].

The emergence of antibiotic resistant bacteria has created an argent need for alternative antimicrobial strategies. Coupling semiconductors with complementary band alignment has proven effective in enhancing antibacterial activity by facilitating electron-hole separation, suppressing recombination, and promoting interfacial charge tranfers [7-11]. This process enables efficient generation of reactive oxygen species (ROS) which play crucial role in microbial inactivation under light irradiation [12-14]. Several semiconductor combination such as TiO_2–WO_3, WO_3–SiO_2 [16–17], TiO_2–CeO_2 [20], TiO_2–Fe_2O_3 [21], and WO_3–$BiVO_4$ [26–27], have been reported for antibacterial application. TiO_2 and WO_3 are especially notable due to their photoactivity, durability,chemical stability, and large surface area [28-29].

In this study, WO_3/TiO_2 nanocomposites calcined at 800°C and 1200°C were investigated against *Streptococcus mutans, Bacillus subtilis, Echerichia coli, Salmonella typhi*. Unlike prior works focussing on *Staphylococcus aureus and Klebisella pneumoniae* [36-39], this study emphasizes *S.mutans and S.typhin* show enhanced antibacterial activity, particularly at 1200°C attributed to improved crystalline and ROS mediated bacterial inactivation [40-42].

2. Synthesis

All the chemicals of AR grade were purchased from Sigma Aldrich and used without further purification.

2. 1 Preparation of WO_3 & TiO_2 nanoparticles

This **Figure 1** shows the flow chart for the synthesis of WO_3 nanoparticles by the co-precipitation method and TiO_2 nanoparticles by the hydrothermal method, outlining the step-by-step procedures involved in each process

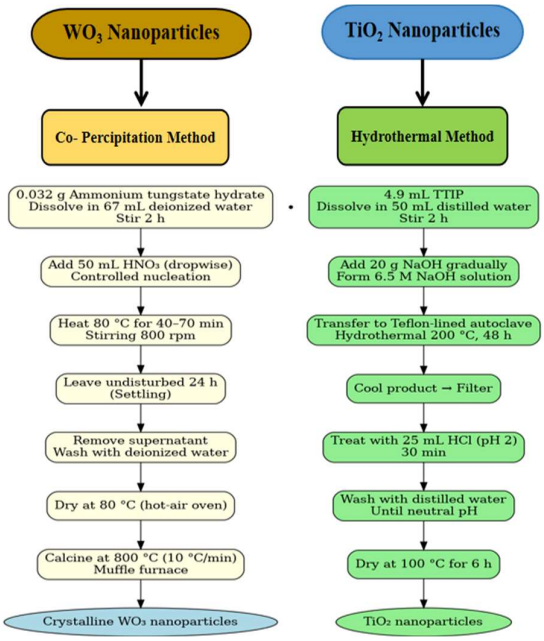

Figure 1: Flow chart for the synthesis of WO_3 and TiO_2 nanoparticles using the co-precipitation and hydrothermal methods.

2.3 Preparation of WO_3/TiO_2 Nanocomposites

The synthesis of WO_3/TiO_2 nanocomposite involved the following steps, following the method described by Pined-Escobar, J.A. **[38]**:

Step 1: Titanium isopropoxide (4.5ml) was mixed with 50 ml of 2-proponal and 5ml of acetic acid, ensuring unifrom dispersion in an acidic medium.

Step 2: Separately, 1 g of WO_3 and 1g of TiO_2 were dispersed in 40ml of 2-propanol and ultrasonicated for 30 min using an ultrasonic probe (VXC 13O, Sonics & Materials, Inc.) to from a homogeneous suspension, which was then slowly introduced into the acidic titanium solution.

Step 3: Hydrolysis waas initiated by adding 5ml deionozed water dropwise, forming a gel- like networks maintained at 70 at 60 mins under stirring and reflux conditions.

Step 4: The obtained WO_3/TiO_2 samples were dried at 100 for 24 hrs to sliminate residual solvent and moisture.

Step 5: .The dried powders were calcined at 800°C and 1200°C for 4h in air. Under light irradiation, WO_3/TiO_2 generates reactive oxygen species that disrupt bacterial membrances, denature proteins, fragment DNA, and inhibit replication, ensuring potent antibacterial activity.

3. Characterizations

Powder X-ray diffraction (XRD) analysis was performed using a Bruker D8 Advance instrument with Cu Kα radiation (λ = 1.5416 Å). The optical bandgap was assessed using an Ocean Optics UV-Vis spectrophotometer, while functional group analysis was conducted with a Perkins Elmer Spectrum 2 Fourier Transform Infrared (FTIR) spectrometer. High-resolution scanning electron microscopy (HRSEM) combined with energy-Dispersive X-ray (EDX) analysis was carried out on an FEI Quanta 200 instrument, operated at 25 kV, to examine the morphology and elemental composition of the prepared powders **[39].**

4. Antibacterial Assay

The antibacterial evaluation of the WO_3/TiO_2 nanocomposites heat-treated at 800°C and 1200°C was conducted using disc diffusion and Muller-Hinton Agar (MHA) methods. The study focused on both Gram-positive strains, namely *Streptococcus mutans* and *Bacillus subtilis*, as well as Gram-negative strains, specifically *Escherichia coli* and *Salmonella typhi*. The methodologies employed allowed for the measurement of the inhibition zones around the nanocomposite discs, providing quantitative data on the antibacterial efficacy of the materials. Further insights into the antibacterial performance and its relevance are provided in the Results and Discussion section.

5. Results and Discussion

5.1 Powder XRD Analysis

Figure (2a-2d) presents the X-ray diffraction (XRD) patterns of WO_3, TiO_2, and WO_3/TiO_2 nanocomposites calcined at 800°C and 1200°C. The WO_3 sample **(Figure 2a)** crystalline in the monoclinic phase, as confrimed by diffraction peaks matching JCPDS No. 083-0950, with prominent reflection at 2θ values of 23.1°, 23.5°, 24.3°, 33.2°, 41.4°, 49.9°, and 50.3°, indexed to the (002), (020), (200), (022), (202), (222), (400), and (114) planes, respectively. The calculated lattice parameters (a = 7.613 Å, b = 7.455 Å, c = 7.269 Å) align well with reported monoclinic WO_3 structures [30]. Similarly, the TiO_2 sample (Figure 2b) exhibit distinst peaks consistent with the rutile phase, verified by JCPDS No. 75-1537. The diffraction maxima observed at 2θ = 27.4°, 36.0°, 39.2°, 41.2°, 44.0°, 54.3°, 56.6°, 62.7°, 64.0°, 65.3°, and 69.0° correspond to the (110), (101), (200), (111), (210), (211), (220), (002), (310), (221), and (301) planes, and the rutile TiO_2 phase exhibites lattice constants of a = 4.565 Å, b = 4.568 Å, and c = 3.776 Å. Crystallite size calculated using the Scherrer equation were 42 nm for WO_3 and 87 nm for TiO_2 confirming the formation of well-defined crystalline structure. For the WO_3/TiO_2 nanocomposites (Figures 2c-2d), the XRD pattern confirm the coexistence of rutile TiO_2 and monoclinic WO_3 phases without detectable impurities, exhibitin > 90% crystallinity. Such high structure integrity is essential for antibacterial activity [40-41], as the stable, well crystalline, and high-surface-area structure promotes efficient ROS generation and enhances interaction with bacterial cells.

The structure insight provided by XRD are further supported by the WO_3,TiO_2 and WO_3/TiO_2 nanocomposites recorded in the 400- 4000 cm^{-1} range **Figure (2e-2h).** For WO_3 broad band at 3370 cm^{-1} corresponds to O-H stretching vibrations,

while peaks at 1615cm^{-1} and 1406 cm^{-1} are assigned to H-O-H bending of adsorbed water [43] and W-O-H vibration confirming surface hydroxyl and water interaction. In TiO_2 O-H stretching appears at 3374 cm^{-1}, the water bending mode is observed at 1640 cm^{-1} and characteristics banf at 481 cm^{-1} corresponds to Ti-O bending and Ti-O vibration, consistent with the structrual stability revealed by XRD [44-46]. The WO_3/TiO_2 nanocomposites display combined vibrational modes of both oxides with a strong O-H stretching band at 2965 cm^{-1} confirming retention of hydroxyl groups a band a 2300 cm^{-1} attributed to atmospheric CO_2 and a deformation band at 1632 cm^{-1} confirming adsorbed water [47]. Importantly a strong W-O-W stretching vibration at 941 cm^{-1} observed in sample calcined at 800°C and 1200°C verifies the incorportion and stabilization of WO_3 within the composites. Together, the XRD and FTIR analyses that the WO_3/TiO_2 nanocomposites possess high crystallinity, stable lattice frameworks and preserved functional groups (hydroxyl, Ti-O, and W-O-W bonds), which not only ensure ensure structural stability but also provide active surface sites for ROS generation. These synergistic structual and vibrational features strongly support the potential of WO_3/TiO_2 nanocomposites as efficient antibacterial materials.

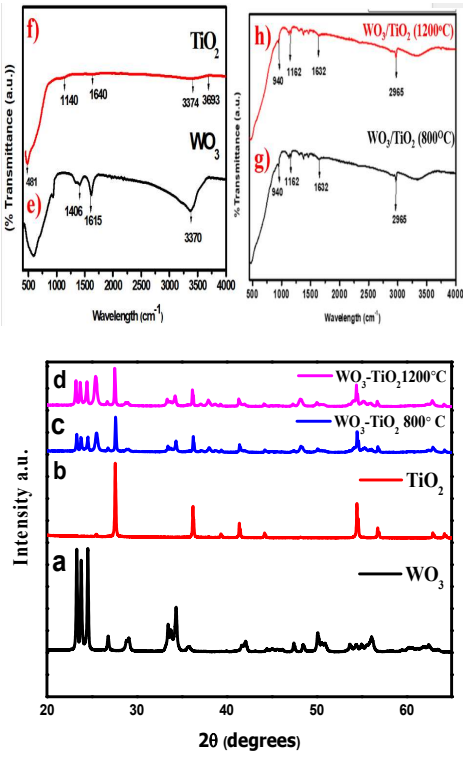

Figure 2. (a–d) XRD patterns of WO_3, TiO_2, and WO_3–TiO_2 nanocomposites calcined at 800 °C and 1200 °C, and (e–h) FTIR spectra of the same samples.

5.2 UV-Visible Analysis

The optical properties of WO_3, TiO_2 and WO_3/TiO_2 nanocomposites were systematically examined using UV-Vis absorption spectroscopy in the wavelenght range of 250 - 800 nm, as presented in **(Figures 3a-3d).** WO_3 displayed a prominent absorption peak at 470 nm, TiO_2 at 495 nm, while the WO_3/TiO_2 nanocomposites calcined at 800°C and 1200°C exhibited peaks at 400 nm and 454 nm, respectively. These absorption features demonstrate the ability of the material to utilize visible light effectively, which is crucial for driving antibacterial processes.

The band gap energies of pure WO_3 and TiO_2 were estimated using the relation

$$Eg = 1240/\lambda$$

Where λ represents the absorption edge. Based on the observed spectra, the bandgap value were calculated as 2.53 eV for WO_3 (470 nm) and 2.7 eV for TiO_2 (495 nm). These values align well with the intrinstic semiconductor properties of the two oxides and confirms their capability as visible-light responsive antibacterial activity [48]. To further understands the electronic behavior of WO_3/TiO_2 composites, the Tauc plot methods was employed, appyling the equation.

$$(\alpha h\nu)^n = A(h\nu - Eg)$$

Where α is the absorption coefficient, hv is photon energy, and Eg is the bandgap energy [48-49]. From this analysis, the composites calcined at 800ºC and 1200ºC were found to possess bandgap of 3.0 eV and 3.15 eV, respectively.

Notable, the slight increase in bandgap with higher calcination temperature is associated with improved photon absorption, better charge separation, and reduced electron- hole recombination.These properties directly enhance ROS production, which induces lipid peroxidation, protein denaturation, and DNA fragmentation in bacterial. Consequently, WO_3/TiO_2 nanocomposites, especially at 1200ºC exhibit superior antibacterial activity through efficient ROS-mediated disinfection.

Figure 3: UV- Visible spectroscopy for **(a)** WO_3, (b)

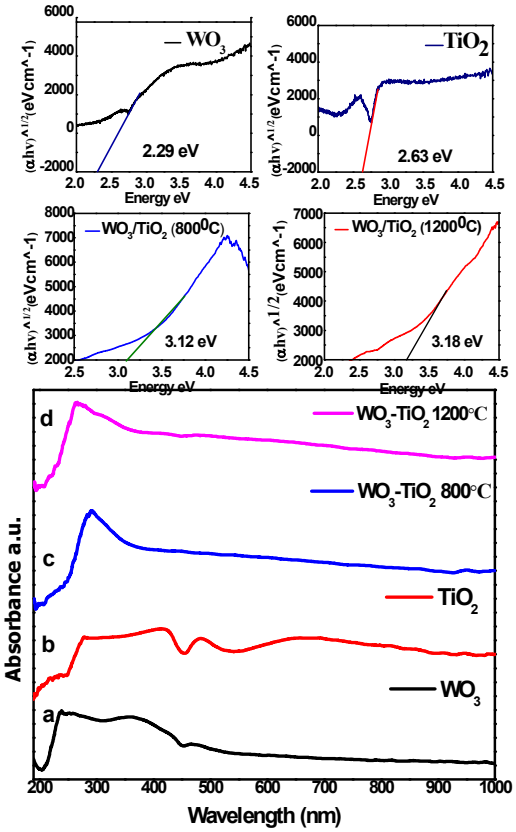

TiO_2 and (c) WO_3-TiO_2 (800 ºC) and (d) WO_3-TiO_2 (1200ºC).

5.3 HR-SEM Analysis

Figure 4(a-h) presents the High-Resolution Scanning Electron Microscopy (HR-SEM) images and Energy Dispersive X-ray (EDX) spectra of pure WO_3,TiO_2, and WO_3/TiO_2 nanocomposites subjected to thermal treatment. The HR-SEM micrograph **(Figure 4a-4d)** clearly indicate that the particles exhibit a range of sizes with noticeable agglomeration, which is typical for nanoparticle system due to their high surface energy. Pure WO_3 **(Figure 4a)** appears as regular nanoparticles with approximate dimension of 500 nm in length and width, forming a relatively uniform morphology. In contrast, the HR-SEM images of WO_3/TiO_2 nanocomposites **(Figure 4b-4d)** reveals nearly spherical nanoparticles with an average diameter of 31 nm. The nanocomposites are densely packed and interconnected, with increased agglomeration attributes to high tempaerature calcination at 800°C and 1200°C. This thermal treatment promotes grain growth, densification, and reduced porosity, which collectively enhance surface area and facilitate improved charge tranfers factor crucial for antibacterial activity. These structure feartures strengthen surface interaction and ROS generation, thereby improving antibacterial performances.

The corresponding EDX spectra **(Figure 4e-4h)** further confirm the successful synthesis and compositional purity of the samples. The spectra clearly identify the characteristic elemental peaks of tungsten (W), titanium (Ti), and oxygen (O), which are unifromly distributed across the nanocomposites. The absence of foreign element such as carbon or other contaminants highlight the high purity of the synthesized WO_3/TiO_2 composites. Moreover, the EDX spectra of nanocomposites treated at 800°C and 1200°C **(Figure 4g-4h)** display no significant peak shift, indicating that the thermal treatment maintains structural integrity while promoting close interfacial contact between WO_3 and TiO_2. Thus, the combined HR-SEM and EDX analyses provide critical insight into the optimized morphology composition, and purity of WO_3/TiO_2 nanocomposites, underscore their potenial for biological and envirnomental applications.

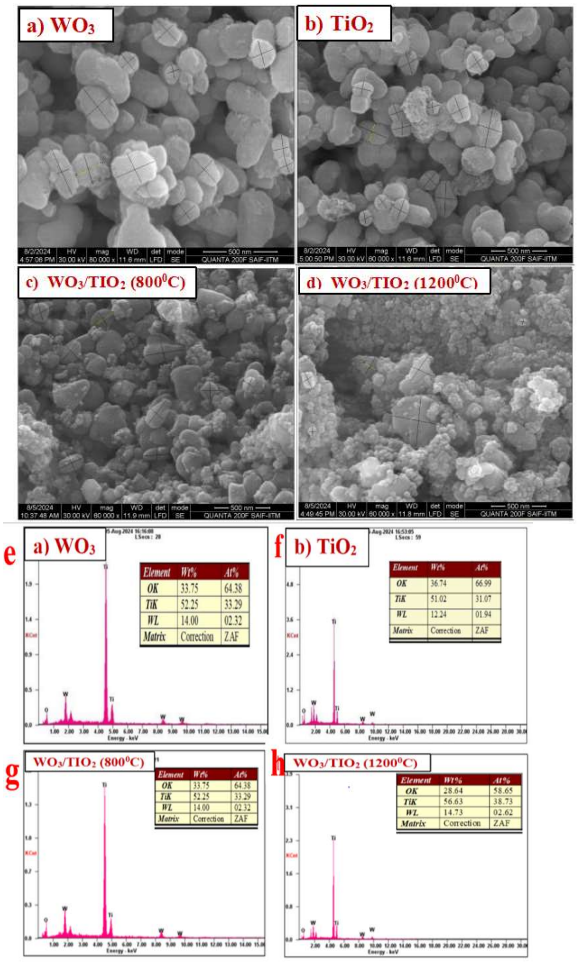

Figure 4: HRSEM analysis (a) WO_3 (b) TiO_2 (c) WO_3-TiO_2 (800 ºC), (d)WO_3-TiO_2 (1200ºCFigure 6: EDX Spectra (e) WO_3, (f) TiO_2, (g) WO_3-TiO_2 (800ºC), (h) WO_3-TiO_2 (1200ºC),

6. Antibacterial Activity Evaluation

The antibacterial activity of WO_3/TiO_2 nanocomposites was evaluted using the agar diffusion methods on Muller-Hinton Agar (MHA) medium againts Gram-positive *(Streptococcus mutans, Bacillus subtilis)* and Gram-negative *(Echerichia coli, Salmonella typhi)* bacteria, with streptomycin as the positive control. MHA was prepared by dissoving 3.8 g of MHA and 2g of agar in 100 ml of distilled water, sterilized, and poured into petri plates. Nanocomposites were serially diluted in nutrient broth, inoculated with bacterial cultures, are incubated for 24 h at 37℃ to determine minimum inhibitory concentration (MIC). Using DMSO as solvent, four concentration (125, 250, 500, and 1000 µl) were tested, while streptomycin (1 mg/ml, 20 µl) as the positive control. The lowest concentration suppressing bacterial growth was noted as the MIC.

Nanocomposites synthesized at 1200℃ displayed greater antibacterial compared to those synthesized at 800 ℃. Inhibition zones expanded from 10-14 mm (800 °C) to 14-20 mm (1200 °C), with *S.typhi* showing the largest increase. Control inhibition zones measured 30-36 mm (800 °C) and 31-36 mm (1200 °C). Enhanced activity at 1200 °C is attributed to improved crystalline, phase formation, and increased ROS generation, leading to stronger bacterial membrances disruption and lower MIC values. These result confirm that higher synthesis temperatures improve antibacterial performance, highlighting WO_3/TiO_2 nanocomposites as promising candidates for medical, envirnomental and industrial application. **Table 1** and **Figure 5** present detailed inhibition zone comparisons.**Table 1:** Comparison of WO_3/TiO_2 nanocomposites for antibacterial activity

Microorganism	**Zone of inhibition in mm**					**References**
	Volumes (µl/ml)				**Streptomycin (control)/ Ampicillin**	
	125	**150**	**500**	**1000**		
Staphylococcus aureus			10	19	27	**[51]**
Bacillus subtilis	-	-	10	14	20	**[52]**
E.coli	-	-	10	16	20	
Salmonella typhi			8	14	19	
E.coli	-	10	11	16	20	**[53]**
Bacillus subtilis	-	-	9	12	20	**[54]**
Salmonella typhi			8	14	10	
E.coil	-	10	11	12	16	**[55]**
E.coli, K.pneumoniae, S. aureus, P.Vulgaris,and P.aeruginosa	-	10	11	12	19	**[56]**
E. coli	-	9	10	14	16	**[57]**
Staphylococcus Mutants (800°C)	9	11	12	13	31	**This work**
E.coil (800°C)	8	11	13	15	36	**This work**
Salmonella typhi (800°C)	0	10	12	14	33	**This work**
Bacillus subtilis (800°C)	10	11	12	15	36	**This work**
S. Mutants (1200°C)	10	11	13	15	31	**This work**
B.Subtilis (1200°C)	10	12	14	18	36	**This work**
E. coli (1200°C)	10	12	13	17	30	**This work**
Salmonella typhi (1200°C)	-	13	15	20	35	**This work**

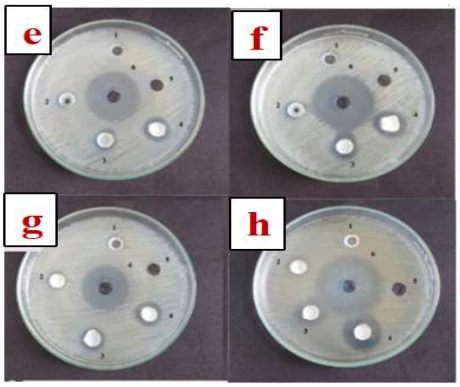

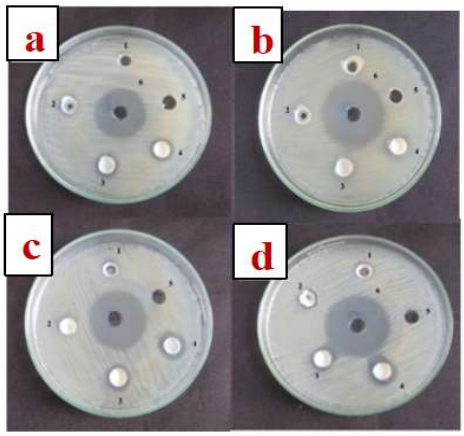

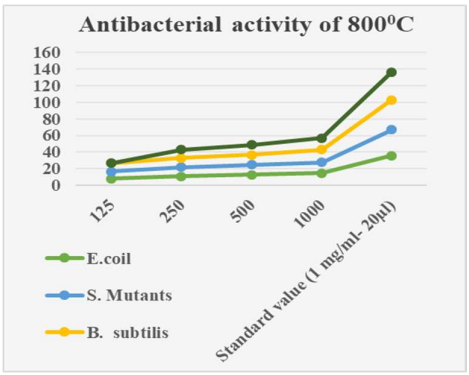

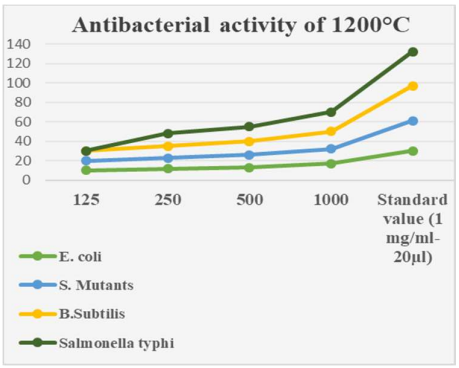

Figure 5: Antibacterial activity of WO_3–TiO_2 nanocomposites calcined at 800 °C against (a) *S. mutans*, (b) *B. subtilis*, (c) *E. coli*, and (d) *S. typhi*, and at 1200 °C against (e) *S. mutans*, (f) *B. subtilis*, (g) *E. coli*, and (h) *S. typhi*, along with **(i)** schematic flow chart illustrating the antibacterial mechanism of WO_3–TiO_2 (800–1200 °C) nanocomposites.

7. ANTIFUNGAL ACTIVITY

In general, the WO_3 andTiO_2 nanocomposites effectively prevent fungal growth, break biofilms and deactivate spores. They generate reactive oxygen species (ROS) that damage critical biological components such as membranes, protein, lipids, and nucleic acids, leading to fungal cell death or growth retardation. Furthermore, the capacity to dissolve biofilms structures increases treatment efficacy and inhibits spore germination, making these nanocomposites especially beneficial against drug-resistant fungal strains **[39-40]**.

The co-precipitate synthesized WO_3/TiO_2 nanocomposites at 800°C and 1200°C were subjected to antifungal treatment against *Candida albicans* and *Aspergillus niger* using the zone of inhibition (ZOI) methods **[41]**. **Figure 6** show the degree of the antifungal activity in the clear zones surrounding the sample wells. **Table 1** presents a quantitative summary of the result obtained.**Table 1:** literature survey of WO_3/TiO_2 Nanocomposites for antifungal activity

Microorganism	**Zone of inhibition in nm**						
	100 µg	**200 µg**	**400 µg**	**600 µg**	**Standard (1mg/ml-20 µl)**	**References**
Aspergillus niger-MTCC-282 TCW 0.75 h	0	11 ± 0.40	23 ± 0.25	19± 0.41	32 ± 0.25	

Microorangism	**150 µg**	**250 µg**	**500 µg**	**1000 µg**	**Standard (1mg/ml-20 µl)**	**Current Research work**
Aspergillus niger-MTCC-282 TCW 0.75 h	0	15 ± 0.25	28±0.25	22± 0.35	32± 0.25	
Candida albicans (800)	0	12	14	15	20	**Current work**
Aspergillus niger (800)	-	-	-	-	10	
Candida albic	14	15	16	18	30	

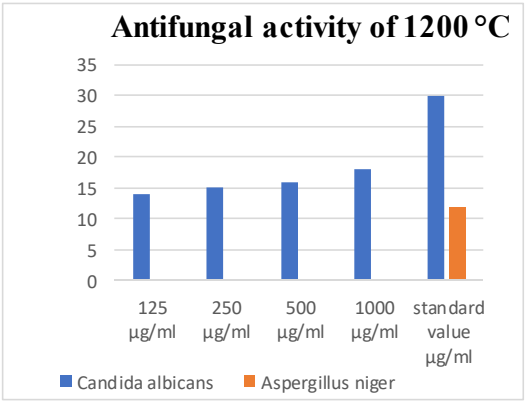

ans (1200)						
Aspergillus niger (1200)	-	-	-	-	12	

From literature review, the *Aspergillus niger* (MTTCC-282 TC) had a maximal inhibition zone of (11-23nm) at 1 mg/ml-20L at lower concentration (100 µg) for control at 32 nm. However at modified condition (MTTCC-282 TC W 0.75h) there is a slight increase in inhibition was observed at 15-28 nm (37) under same concentration. In the present study, the prepared nanocomposites at 800°C reveals the moderate inhibition against *Candida albicans* (10-15 nm) whereas, inhibition against *A. niger* was ineffective. In contrast, nanocomposites synthesized at 1200°C shows better inhibitory zones (14-18 nm) for *Candida albicans* closer to standard medication efficacy and it shows moderate activity (12 nm) for *A. niger*. Perhaps, *Candida Albicans* shows greater susceptibility than *A. niger*, due to differences in cell wall composition. Compared with the previously reported data **[41]** the results of WO_3/TiO_2 nanocomposites synthesized at 800°C and 1200°C have higher antifungal activity. The samples prepared at 1200°C show better inhibitory zones compared with the samples at 800°C signifies the synthesis temperature has an impact on antifungal efficiency for the present work. Higher temperatures also improve ROS generation, charge separation, and structural properties, which boost membrane disruption **[42- 43]**.

Figure 6: Antifungal performances of WO_3/TiO_2 Nanocomposites treated at 800°C and 1200°C

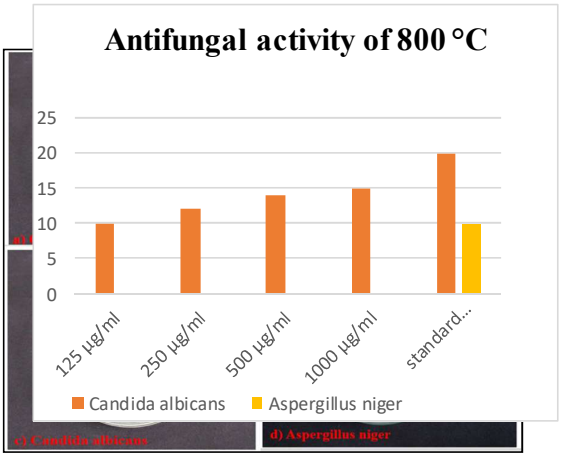

Figure 7: Schematic depicting the antifungal efficacy of WO_3/TiO_2 nanocomposites at 800°C and 1200°C.

8. Conclusion

WO_3/TiO_2 nanocomposites were successfully synthesized by the co-precipitation method and calcined at 800 °C and 1200 °C. XRD confirmed the formation of monoclinic WO_3 and rutile TiO_2 phases with crystallite size of 42 nm and 87 nm. HRSEM revealed spherical nanoparticles (31 nm), while EDX confirmed the unifrom distribution of W, Ti, and O elements. ftir analysis showed the presence of surface hydroxyl groups, and UV- Visible studies indicated visible- light absorption with band gap energies of 3.00 ev and 3.15 eV for the composites calcined at 800°C and 1200°C respectively. The WO_3/TiO_2 nanocomposites exhibited excellent antibacterial activity against Streptococcus mutans, Bacillus subtilis, Escherichia coli, and Salmonella typhi, as well as strong antifungal activity against Candida albicans and Aspergillus niger, with the 1200°C calcined sample showing the highest inhibition. The enhanced antimicrobial performance is attributed to improved crystallinity and increased reactive oxygen species (ROS) generation, which effectively damages microbial cell membranes and intracellular components. These findings demonstrate that WO_3/TiO_2 nanocomposites are promising eco-friendly antimicrobial materials for biomedical applications, environmental disinfection, water treatment, and antimicrobial coatings

REFERENCES

[1]. Khan, Y., et al. "*Nanomaterials for Environmental Remediation: A Review.*" *Environmental Science Nano*, (2019) .6(1), 45-67. DOI: 10.1039/C8EN00745G.

[2]. Zhang, X., et al. "*Recent Advances in Nanocomposites for Photocatalytic Applications.*" *Applied Catalysis B: Environmental*, (2020). 263, 118339. DOI: 10.1016/j.apcatb.2019.118339.

[3]. Rai, M., et al. "*Antimicrobial Nanomaterials: Applications and Future Directions.*"

Nanotechnology in Medicine, 15(3), 159-173. (2018**).** DOI: 10.1007/s12951-018-0864-7.

[4]. Duan, J., et al. . "*Nanocomposites for Water Treatment: A Review." Journal of Hazardous Materials,* 403, 123674 (2021). DOI: 10.1016/j.jhazmat.2020.123674.

[5]. Ocampo, L., et al. "*Nanomaterials in Photocatalytic Water Treatment: Review of Current Progress and Future Perspectives." Chemical Engineering Journal*, 323, 57-78. (2017).DOI: 10.1016/j.cej.2017.04.039.

[6]. Sharma, A., et al. .*"Nanocomposites for Antimicrobial Applications: Recent Advances and Future Perspectives." Journal of Nano biotechnology,* 18, 50. (2020)DOI: 10.1186/s12951-020-05881-4.

[7]. Zhao, X., et al. *Applied Surface Science,* 436, 26-45. (2018).DOI: 10.1016/j.apsusc.2017.11.046.

[8]. Jiang, Y., et al. .*Principles and Perspectives." Materials Today Energy*, 16, 100431.(2020). DOI: 10.1016/j.mtener.2020.100431.

[9]. Gao, Y., et al. " *Catalysis Today*, 318, 123-130. (2019).DOI: 10.1016/j.cattod.2018.10.021.

[10]. Kumar, R., et al. *Chemical Engineering Journal*, 404, 126765. (2021).DOI: 10.1016/j.cej.2020.126765.

[11]. Li, Q., et al. "Heterojunction Photocatalysts: *A Review on Their Preparation and Applications*." *Journal of Alloys and Compounds*, 795, 122-132. (2019). DOI: 10.1016/j.jallcom.2019.06.091.

[12]. D Yiamsawas, K. Boonpavanitchakul, W. Kangwansupamonkon, *Preparation of ZnO nanostructured by solvothermal method,* J. Microsc. Soc. Thail. 23 (2009) 75–78.

[13]. Balachandran S, N. Prakash, K. Thirumalai, M. Muruganandham, M. Sillanpaa, M. Swaminathan, Ind. Eng. Chem. Res. 53 (2014) 8346–8356.

[14]. S. Balachandran, M. Swaminathan, *The simple, template free synthesis of a Bi_2S_3-ZnO heterostructure and its superior photocatalytic activity under UV-A light, Dalton Trans 42* (2013) 5338–5347.

[15]. H.K. Shon, S. Phuntsho, S. Vigneswaran, *Effect of photocatalysis on the membrane hybrid system for wastewater treatment, Desalination* 225 (2008) 235–248.

[16]. R.J. Davis, Z. Liu, Titania-silica: *a model binary oxide catalyst system, Chem. Mater*. 9 (1997) 2311–2324.

[17]. Z. Liu, R.J. Davis, *Investigation of the structure of micro porous Ti-Si mixed oxides by X-ray, UV reflectance, FT-Raman, and FT-IR spectroscopes,* J. Phy.l Chem. 98 (1994) 1253–1261.

[18]. J. Göttsche, A. Hinsch, V. Wittwer, *Electrochromic mixed WO 3 -TiO 2 thin films produced by sputtering and the sol-gel technique: a comparison, Sol. Energy Mater. Sol. Cells.* 31(1993) 415–428.

[19]. I. Shiyanovskaya, M. Hepel, *Bicomponent WO 3 /TiO 2 films as photoelectrodes, J.Electrochem.* Soc. 146 (1999) 243–249.

[20]. D. Camino, D. Deroo, J. Salardenne, N. Treuil, (CeO_2) x-(TiO_2)1-x: *counter electrode materials for lithium electrochromic devices, Sol. Energy Mater. Sol. Cells*. 39 (1995) 349–366.

[21]. Y. Wu, L. Hu, Z. Jiang, Q. Ke, *Study on the electrochemical properties of Fe_2O_3–TiO_2 films prepared by sol-gel process, J. Electrochem. Soc.* 144 (1997) 1728–1733.

[22]. S.K. Poznyak, D.V. Talapin, A.I. Kulak, *Structural, optical, and photoelectrochemical properties of nanocrystalline TiO_2-In_2O_3 composite solids and films prepared by sol-gel method, J. Phy. Chem. B.* 105 (2002) 4816–4823.

[23]. D. Liu, P.V. Kamat, *Photoelectrochemical behavior of thin CdSe and coupled TiO2/CdSe semiconductor films, J. Phy. Chem* 97 (1993) 10769–10773.

[24]. R. Suarez, P.K. Nair, P.V. Kamat, *Photoelectrochemical behavior of Bi_2S_3 nanoclusters and nanostructured thin films*, Langmuir 14 (1998) 3236–3241.

[25]. K.H. Yoon, J. Cho, D.H. Kang, *Physical and photoelectrochemical properties of the TiO_2-ZnO system, Mater*. Res. Bull. 34 (1999) 1451–1461.

[26]. J. Su, L. Guo, N. Bao, C.A. Grimes, *Nanostructured WO_3/$BiVO_4$ heterojunction films for efficient photoelectrochemical water splitting*, Nano Lett 11 (2011) 1928–1933.

[27]. H. Fan, D. Wang, Z. Liu, T. Xie, Y. Lin, *Self-assembled $BiVO_4$/Bi_2WO_6 micro spheres: synthesis, photo induced charge transfer properties and photocatalytic activities*, Dalton Tran 44 (2015) 725–11731.

[28]. S. Noimark, C.W. Dunnill, I.P. Parkin, *Shining light on materials- a self-sterilising revolution, Adv.* Drug Deliv. Rev. 65 (2013) 570–580.

[29]. P. Wu, J.A. Imlay, J.K. Shang, *Mechanism of Escherichia coli inactivation on palladium-modified nitrogen-doped titanium dioxide, Biomaterials* 31 (2010) 7526–7533.

[30]. C. Green-Ruiz*, Adsorption of mercury(II) from aqueous solutions by the clay mineral montmorillonite,* Bull. Environ.Contam. Toxicol. 75 (2005) 1137–1142.

[31]. C. Green-Ruiz, *Effect of salinity and temperature on the adsorption of Hg (II) from aqueous solutions by a Ca-montmorillonite, Environ. Technol*. 30 (2009) 63–68.

[32]. Y. Fernandez-Nava, M. Ulmanu, I. Anger, E. Maranon, L. *Castrillon, Use of granular bentonite in the removal of mercury (ii), cadmium (ii) and lead (ii) from aqueous solutions, Water Air Soil Pollut.* 215 (2010) 239–249.

[33]. D.M. Chen, Q. Zhu, F.S. Zhou, X.T. Deng, F.T. Li, *Synthesis and photocatalytic performances of the TiO_2 pillared montmorillonite, J. Hazard*. Mater. 235 (2012) 186–193.

[34]. Z.S. Sun, Y.X. Chen, Q. Ke, Y. Yang, J. Yuan, *Photocatalytic degradation of a cationic azo dye by TiO_2 /bentonite nanocomposite, J. Photochem. Photobiol*. A 149 (2002) 169–174.

[35]. K. Thirumalai, E.T. Deva Kumar, R. Aravindhan, J. Raghava Rao, M. Swaminathan, *Hierarchically structure d b entoniteloade d Bi_2O_3 - ZnO and its multiple applications, Surf. Interfaces 5* (2016) 30–38.

[36]. Kusiak-Nejman, E., Wanag, A., Kapica-Kozar, J., Morawski, A.W., & Zaleska-Medynska, A. The Effect of Calcination Temperature on Structure and Photocatalytic Properties of WO_3/TiO_2 Nanocomposites. *Journal of Nanomaterials*, *2016*, Article ID 3145912. https://doi.org/10.1155/2016/3145912.

[37]. Liu, Y., Liu, L., & Zhang, Y. Composition Directed Generation of Reactive Oxygen Species in Hybrid TiO_2 Nanoparticles. *ACS Applied Materials & Interfaces*, *7*(24), 13304–13314. (2015). https://doi.org/10.1021/acsami.5b03626.

[38]. Ali, H., Guler, A.C., Masar, M., Urbanek, P., Urbanek, M., Skoda, D., Suly, P., Machovsky, M., Galusek, D., &Kuritka, I. Solid-State Synthesis of Direct Z-Scheme Cu_2O/WO_3 Nanocomposites with Enhanced Visible-Light Photocatalytic Performance. *Catalysts*, *11*(2), 293.(2021). https://doi.org/10.3390/catal11020293.

[39]. Sato, T., & Katayama, M. Indoor-Light-Activated Blue TiO_2-Molecule-WO_3 Visible-Light Photocatalyst Complex for Efficient Sterilization. *ACS Omega*, *8*(17), 15023–15031. (2023).https://doi.org/10.1021/acsomega.3c00856.

[40]. Gopinath,K.P., Madhav, N.V., Krishnan, A., Malolan, R., & Rangarajan, G. . Bio material (Garlic and Chitosan)-Doped WO_3-TiO_2 Hybrid Nanocomposite for Visible Light Photocatalytic Degradation of Ciprofloxacin and Antimicrobial Activity. *ACS Omega*, *5*(49), 31768–31781. (2020)https://doi.org/10.1021/acsomega.0c04154

[41]. Güler, A.C., Ali, H., &Kuritka, I. Enhancement of Photocatalytic Antimicrobial Performance via Dye-Sensitized TiO_2 Nanomaterials: A Review. *Scientific Engineering and Environmental Sciences*, *6*(2), 399–413. (2021). https://www.sciltp.com/journals/see/article/download/399/313/2979.

[42]. Martínez-de la Cruz, A., Sánchez-Martínez, D., & Cuéllar, E. L. *Synthesis and characterization of WO_3 nanoparticles prepared by the precipitation method: Evaluation of photocatalytic activity under vis-irradiation.Solid State Sciences*, *12*(1), 88–94. (2010). https://doi.org/10.1016/j.solidstatesciences.2009.10.010.

[43]. Sanchez-Martinez, A., Koop-Santa, C., Ceballos-Sanchez, O., López-Mena, E. R., González, M. A., Rangel-Cobián, V., Orozco-Guareño, E., & García-Guaderrama, M. *Study of the preparation of TiO_2 powder by different synthesis methods.Materials Research Express*, *6*(8).(2019). https://doi.org/10.1088/2053-1591/ab21e8.

[44]. Pinedo-Escobar, J. A., Junpeng Fan, Edgar Moctezuma, Gomez-Solís, C., Martinez, C. J. C., & Gracia-Espino, E. Nano particulate *double-heterojunction photocatalysts comprising TiO_2(Anatase)/WO_3/TiO_2(Rutile)with enhanced photocatalytic activity toward the degradation of methyl orange under near-ultraviolet and visible light.ACS Omega*, *6*(18), 11840–11848. (2021). https://doi.org/10.1021/acsomega.0c06054.

[45]. M. Huang, S. Yu, B. Li, D. Lihui, F. Zhang, M. Fan, L. Wang, J. Yu, C. Deng, *Influence of preparation methods on the structure and catalytic performance of SnO_2-doped TiO_2 photocatalysts,* Ceram. Int. 40 (2014) 13305–13312.

[46]. Filippo E, Carlucci C, Capodilupo A L ,Perulli P , Conciauro F, Corrente G A , Gigli G and Ciccarell G, *Enhanced Photocatalytic Activity of Pure Anatase TiO_2 and Pt-TiO_2 Nanoparticles Synthesized by Green Microwave Assisted Route, Materials Research* 18(3) pp 2015. 473-481.

[47]. Mohammed B A and Ahmed L M *Improvement the Photo Catalytic Properties of ZnS nanoparticles with Loaded Manganese and Chromium by Co-Precipitation Method Journal of Global Pharma Technology* 10(7) pp 2018. 129-138.

[48]. Ahmed L M, Hussen F H and Mahdi A *Photocatalytic Dehydrogenation of Aqueous Methanol Solution by Naked and Platinized TiO_2 Nanoparticles Asian Journal of Chemistry* 24(12) pp 2012. 5564-5568.

[49]. B. Boga, I. Székely, Z. Pap, L. Baia, M. Baia, *Detailed Spectroscopic and Structural Analysis of TiO_2/WO_3 Composite Semiconductors*. J. Spectrosc. 2018, 2018, 1–7.

[50]. C. Kang, L. Jing, T. Guo, H. Cui, J. Zhou, H. Fu, *The Journal of Physical Chemistry C* 2008, 113, 1006–1013.

[51]. H. Nogueira, A. Cavaleiro, J. Rocha, T. Trindade, J. de Jesus, Mater. Res. Bull. D. P. ***Mater***. ***Res***. ***Bull***. ***2004 39,***683–693.

[52]. L. Paula, M. Hofer, V. Lacerda, D. Bahnemann, A. Patrocinio, ***Photochemical*** & Photobiological Sciences ***2019***, ***18*** (10).

[53]. Kumar, P. M.; Badrinarayanan, S.; Sastry, M. *Nanocrystalline TiO_2 studied by optical, FTIR and X-ray photoelectron spectroscopy:correlation to presence of surface states. Thin Solid Films* 2000, 358,122−130.

[54]. Rastogi, L.; Arunachalam, J. *Green synthesis route for the size controlled synthesis of bio compatible gold nanoparticles using aqueous extract of garlic Allium sativum. Adv. Mater. Lett*. 2013, 4, 548−555.

[55]. Tahir, M. B.; Farman, S.; Rafique, M.; Shakil, M.; *Khan, M. I.;Ijaz, M.; Mubeen, I.; Ashraf, M.; Nadeem Riaz, K. Photocatalytic performance of hybrid WO_3 /TiO_2 nanomaterials for the degradation of methylene blue under visible light irradiation.* Int. J. Environ. Anal.Chem. 2019, 1−13.

[56]. F.A. Mir, S. Rehman, K. Asokan, S.H. Khan, G.M. Bhat, *J. Mater. Sci.: Mater. Electron. 25,* 1258–1263 (2014).
[57]. Dhanalekshmi, K. I., Umapathy, M. J., Magesan, P., & Zhang, X. *Biomaterial (Garlic and Chitosan)-Doped WO_3 -TiO_2 Hybrid Nanocomposites: Their Solar Light Photocatalytic and Antibacterial Activities. ACS Omega*, *5*(49), 31673–31683. (2020). https://doi.org/10.1021/acsomega.0c04154.